

Sorted Convolutional Network for Achieving Continuous Rotational Invariance

Hanlin Mo and Guoying Zhao, *Fellow, IEEE*

Abstract—The topic of achieving rotational invariance in convolutional neural networks (CNNs) has gained considerable attention recently, as this invariance is crucial for many computer vision tasks such as image classification and matching. In this letter, we propose a Sorting Convolution (SC) inspired by some hand-crafted features of texture images, which achieves continuous rotational invariance without requiring additional learnable parameters or data augmentation. Further, SC can directly replace the conventional convolution operations in a classic CNN model to achieve its rotational invariance. Based on MNIST-rot dataset, we first analyze the impact of convolutional kernel sizes, different sampling and sorting strategies on SC's rotational invariance, and compare our method with previous rotation-invariant CNN models. Then, we combine SC with VGG, ResNet and DenseNet, and conduct classification experiments on popular texture and remote sensing image datasets. Our results demonstrate that SC achieves the best performance in the aforementioned tasks.

Index Terms—Rotational invariance, convolutional neural network, sorting, interpolation.

I. INTRODUCTION

FEATURE extraction is one of the core tasks in computer vision and pattern recognition. An ideal feature should be invariant to various spatial deformations caused by imaging geometry, which ensures that it captures intrinsic information of an image. For many practical applications, such as object recognition, image classification, and patch matching, two-dimensional rotation is the most common spatial transformation, and thus it is essential to achieve rotational invariance of image features in these cases.

In past decades, numerous hand-crafted features that are invariant to image rotation have been developed [1], [2], [3], [4], [5], [6]. Since 2012, deep neural networks, especially convolutional neural networks (CNNs), have been proven to be more effective than most hand-crafted features in computer vision tasks. Nonetheless, conventional convolution operations are not rotation-invariant. Actually, even if an image is slightly rotated, CNNs may not be able to recognize it correctly. To address this, a direct approach is to train a CNN with rotated training samples, i.e. data augmentation. However, it has obvious drawbacks, including increasing training time and costs, learning some redundant weights, and further reducing the interpretability of CNNs [7], [8].

This work was supported in part by the National Natural Science Foundation of China (Grant No.60873164, 61227802 and 61379082) and the Academy of Finland for Academy Professor project EmotionAI (Grant No.336116). (Corresponding author: Guoying Zhao.)

The authors are with the Center for Machine Vision and Signal Analysis, University of Oulu, 90014 Oulu, Finland (e-mail: hanlin.mo@oulu.fi; guoying.zhao@oulu.fi).

Hence, recent research has aimed to incorporate rotational invariance into convolutional operations and design new network architectures. Based on various methods, such as orientation assignment, polar/log-polar transform, steerable filters, and multi-orientation feature extraction, researchers successively propose Spatial Transformer Network (STN) [9], Polar Transformer Network [10], General E(2)-Equivariant Steerable CNN (E(2)-CNN) [11], Group Equivariant Convolutional Network (G-CNN) [12], Rotation Equivariant Vector Field Network (RotEqNet) [13], Harmonic Network (H-Net) [8], Bessel CNN (B-CNN) [14], Rotation-Invariant Coordinate CNN (RIC-CNN) [15] and so on [16], [17].

However, existing rotation-invariant convolution operations have three major limitations: **1)** Most methods are invariant to specific rotation angles rather than arbitrary angles [12], [13], [16], [17]. Some of them, like RIC-CNN [15], are only invariant to continuous rotations around image center; **2)** Some methods require extra trainable parameters and rely on data augmentation when training [9], [18], [19], [20]; **3)** Many rotation-invariant convolution operations are more complex and not easily replaceable with traditional convolution in common CNN models (like VGG and ResNet) [8], [11], [12], [14]. Moreover, some papers still use data augmentation to train their proposed rotation-invariant CNN models, making it difficult to determine whether the new architectures or only rotated training samples enhanced CNN models' rotational invariance [12], [13].

The goal of this letter is to address these limitations in some extent. Our contributions can be summarized as follows:

- Inspired by some hand-crafted features of texture images [21], [22], [23], we propose a Sorting Convolution (SC) that achieves continuous rotational invariance without additional learnable parameters. By substituting all standard convolutions in a CNN model with the corresponding SC, we can obtain a Sorting Convolutional Neural Network (SCNN).
- We train SCNN on original MNIST training set without data augmentation, evaluate its performance on MNIST-rot test set, and analyze the impact of convolutional kernel sizes, different sampling methods, and sorting strategies on its rotational invariance. In comparison to previous rotation-invariant CNN models, our SCNN achieves state-of-the-art result.
- We integrate SC into widely used CNN models and perform classification experiments on popular texture and remote sensing image datasets. Our results show that SC significantly increases the classification accuracy of these models, particularly when training data is limited.

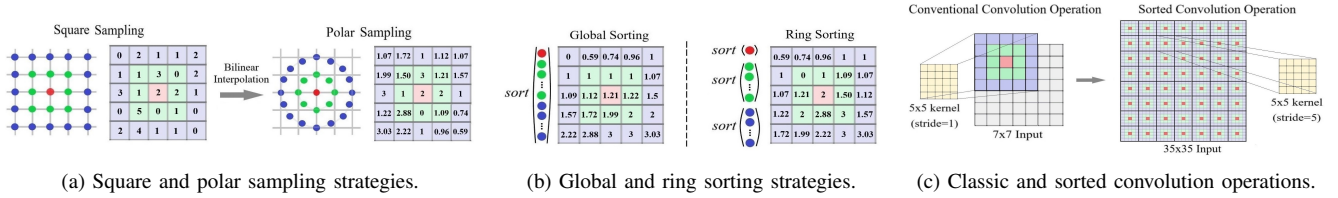


Fig. 1: The implementation details of the proposed sorted convolutional operation.

II. METHODOLOGY

A. Sorted Convolution Operation

For an input $F(X)$ with the size of $h \times w$, a conventional convolutional operation Φ_C acting on a given point $X_0 \in \{1, 2, \dots, h\} \times \{1, 2, \dots, w\}$ can be expressed as below

$$\Phi_C(X_0, F(X)) = \sum_{P \in \mathcal{S}} W(P) \cdot F(X_0 + P) \quad (1)$$

Here, W is a $(2n + 1) \times (2n + 1)$ learnable kernel, n is a non-negative integer, and P enumerates all points on the square grid $\mathcal{S} = \{-n, -n + 1, \dots, n\} \times \{-n, -n + 1, \dots, n\}$. For example, when W is a 3×3 kernel, we have $\mathcal{S} = \{(-1, -1), (-1, 0), \dots, (0, 1), (1, 1)\}$, which contains 9 points. Our paper only considers odd-sized W because the shift issue occurs in even-sized ones [24].

Assuming that $G(Y)$ is a rotated version of $F(X)$, that is, $G(Y) = F(R_{-\theta}Y)$, where $R_{-\theta}$ is a 2×2 rotation matrix and θ represents the rotation angle. Let Y_0 be the corresponding point of X_0 , then the convolution operation at Y_0 is

$$\Phi_C(Y_0, G(Y)) = \sum_{P \in \mathcal{S}} W(P) \cdot G(Y_0 + P) \quad (2)$$

Since $X_0 = R_{-\theta}Y_0$, the following relation can be obtained

$$G(Y_0 + P) = F(R_{-\theta}(Y_0 + P)) = F(X_0 + R_{-\theta}P) \neq F(X_0 + P) \quad (3)$$

By substituting (3) into (2), we can find

$$\Phi_C(Y_0, G(Y)) \neq \Phi_C(X_0, F(X)) \quad (4)$$

Thus, the conventional convolutional operation Φ_C is not invariant to two-dimensional rotation.

Assuming that $(2n + 1) \cdot (2n + 1)$ points $R_{-\theta}P$ still belong to the square grid \mathcal{S} , that is, after rotation, all $R_{-\theta}P$ and P completely overlap. In this case, although $G(Y_0 + P) \neq F(X_0 + P)$, we have

$$\begin{aligned} \{G(Y_0 + P)\}_{P \in \mathcal{S}} &= \{F(X_0 + R_{-\theta}P)\}_{P \in \mathcal{S}} \\ &= \{F(X_0 + P)\}_{P \in \mathcal{S}} \end{aligned} \quad (5)$$

meaning that the input values used for the convolution operation at points X_0 and Y_0 are the same, but with different arrangements. Obviously, if the $(2n + 1) \cdot (2n + 1)$ values in $\{G(Y_0 + P)\}_{P \in \mathcal{S}}$ and $\{F(X_0 + P)\}_{P \in \mathcal{S}}$ are sorted in ascending order separately, the two resulting sorted sequences should be exactly the same.

If we arrange the sorted sequence in row-major order on the $(2n + 1) \times (2n + 1)$ square grid \mathcal{S} , and represent the new

value at point P after sorting as $F^s(X_0 + P)$. Then, the sorted convolution operation can be defined as follows

$$\Phi_{SC}(X_0, F(X)) = \sum_{P \in \mathcal{S}} W(P) \cdot F^s(X_0 + P) \quad (6)$$

Since $F^s(X_0 + P) = G^s(Y_0 + P)$ for any P , we have

$$\Phi_{SC}(Y_0, G(Y)) = \Phi_{SC}(X_0, F(X)) \quad (7)$$

indicating that Φ_{SC} is invariant to arbitrary rotations. Moreover, the sorting operation does not require learning from the training data, so the number of learnable parameters in Φ_{SC} is the same as in the standard convolutional operation Φ_C .

B. Sampling and Sorting Strategies

Formula (5) assumes that all $R_{-\theta}P$ are still on the $(2n + 1) \times (2n + 1)$ square grid \mathcal{S} , which is only true for discrete convolution when $\theta = k \cdot 90^\circ$ (k is an integer). To address this issue, a polar coordinate system centered at X_0 is established, and $8r$ points are evenly sampled on a circumference with radius r centered at X_0 , where $r = 1, 2, \dots, n$ (see Fig. 1(a)). Bilinear interpolation is used to obtain the values of $F(X)$ at these points, which are then sorted in ascending order and arranged row by row on the square grid \mathcal{S} . When the rotation angle $\theta = k \cdot 360^\circ / (8r)$, the $8r$ points on the circle with radius r coincide before and after rotation. Thus, compared to the square sampling, the polar sampling ensures better validity of the formula (5) and rotational invariance of Φ_{SC} .

In addition to the sampling strategy, the sorting strategy is also worth discussing. In fact, the sorting destroys the local structure of $F(X)$ in the $(2n + 1) \times (2n + 1)$ neighborhood of X_0 . Previous researchers also used sorting to construct rotation-invariant features for texture images. To preserve the local structure to some extent and improve the discriminability of features, they designed a ring sorting method [21], [22]. Unlike the global sorting, the ring sorting separately sorts the $8r$ points in the r th square/circular ring about the center point X_0 and arranges the sorted values in a row-first manner at these $8r$ positions (see Fig. 1(b)). The method preserves some spatial information while ensuring rotational invariance.

C. The Implementation of Sorted CNN

The traditional convolution Φ_C (defined in (1)) produces an output with the size of $h \times w$ when the stride is set to 1 and padding is performed. However, for the corresponding Φ_{SC} (defined in (6)), we first sort the input values within a $(2n + 1) \times (2n + 1)$ neighborhood for each position

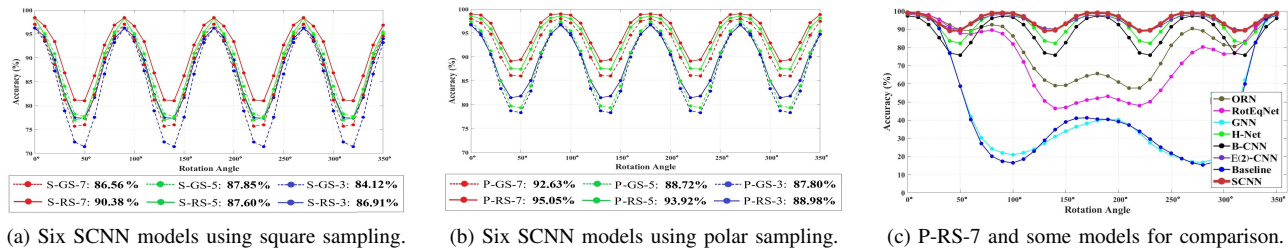


Fig. 2: The classification accuracies from SCNNs and other rotation-invariant CNN models on the MNIST-rot test set.

$X \in \{1, 2, \dots, h\} \times \{1, 2, \dots, w\}$, then concatenate all the sorted neighborhoods to form a new input with size $((2n+1) \cdot h) \times ((2n+1) \cdot w)$. Next, we perform a $(2n+1) \times (2n+1)$ convolution on this input with a stride of $(2n+1)$ and no padding is applied. Obviously, the output size of Φ_{SC} is still $h \times w$, the same as the output of Φ_C , while ensuring rotational invariance. Hence, SC and traditional convolutions can be swapped. By replacing all Φ_C in a standard CNN with the corresponding Φ_{SC} , we can create an SCNN. When the input $F(X)$ is rotated by θ and then input the SCNN, the output of the last SC layer in the SCNN is equal to rotating the corresponding output of the original $F(X)$ by θ . If we use max pooling or average pooling operations to reduce the spatial resolution of the output to 1×1 , the resulting feature is invariant to arbitrary rotations and can be used as input for other network structures, such as fully connected layers.

III. EXPERIMENTS

A. Experiment Setup

Datasets: **MNIST** [24] has 70K 28×28 handwritten digit images (0-9), with 60K for training and 10K for testing. 10K training images are randomly selected for validation. Each of test images are rotated from 0° to 350° every 10° , resulting in 360K rotated test images. The new test set is called *MNIST-rot* and used to verify the SCNN’s rotational invariance. **Outex_TC_00012** [25] contains 24 texture classes and 9120 grayscale images of size 128×128 . For each class, 20 texture surfaces are captured under three lighting conditions (“inca”, “t184” and “horizon”) as training images. Then, they are captured as test images from 8 different rotation angles ($5^\circ \sim 90^\circ$) under “t184” and “horizon” lighting conditions. Thus, the size of the training set is $24 \times 20 \times 3 = 1440$, and the size of the test set is $24 \times 20 \times 2 \times 8 = 7680$. **NWPU-RESISC45** [26] is a dataset for remote sensing image scene classification. It contains 31500 RGB images of size 256×256 divided into 45 scene classes, each class containing 700 images. We resize all images to 128×128 and randomly select 400 images from each class as training images, with the remaining images used as test images. Due to the arbitrary shooting angles, there are rotational variations present in many classes, such as “airplane”, “bridge” and “ground track field”.

Models and Training Protocol: We initially design a baseline CNN model with six convolutional layers, having 32, 32, 64, 64, 128, and 128 channels, respectively. We apply 2×2 max pooling after the second and fourth layers, and use

7×7 average pooling after the final convolutional layer. Then, the feature vector is fed into a fully connected layer with ten units. The kernel size for the last two convolutional layers is 3×3 , while for the first four layers, the kernel size is the same $K \times K$, where $K \in \{3, 5, 7\}$. By replacing each of classical convolution operations in the baseline with the corresponding SC, we can obtain a SCNN model. When implementing SC, we have options for square sampling (S) or polar sampling (P), as well as global sorting (GS) or ring-based sorting (RS). This results in 12 different SCNNs ($\{S, P\} \times \{GS, RS\} \times \{3, 5, 7\}$). For example, P-RS-5 indicates that the first four layers use 5×5 SC with polar sampling and ring sorting. We train all these SCNNs on MNIST training dataset with Adam optimizer, while the initial learning rate is 10^{-4} , multiplied by 0.8 every 10 epochs. The number of epochs and the batch size are 100.

To demonstrate the ease of integrating SC with commonly used CNN models, we select VGG16 [27], ResNet18 [28], and DenseNet40 [29] as baseline models. By replacing all traditional convolution operations in these models with SC, we obtain RI-VGG16, RI-ResNet18, and RI-DenseNet40. All of them are trained on Outex_TC_00012 and NWPU-RESISC45, respectively. Again, the Adam optimizer is used, and the training process involves 100 epochs with a batch size of 10. The initial learning rate is set to 10^{-4} for VGG16, RI-VGG16, ResNet, and RI-ResNet, while it is 10^{-3} for DenseNet and RI-DenseNet. It is reduced by a factor of 0.6 every 10 epochs.

Our experiments are performed on a Tesla V100 GPU (16G) upon Rocky Linux 8.7 system and PyTorch 2.0.0 framework. All models are trained from scratch without using pretrained parameters or data augmentation. This allows us to directly observe the performance improvement brought by SC.

B. Results on MNIST-Rot

First, we test rotational invariance of 12 SCNN models with varying convolutional kernel sizes, sampling and sorting strategies on the MNIST-rot dataset. This test set contains 36 subsets, each containing 10K samples with the same rotation angle θ ($0^\circ, 10^\circ, \dots, 350^\circ$). Fig. 2(a) illustrates the classification accuracy of six SCNNs using square sampling on each subset, while Figure 2(b) displays the accuracy of six SCNNs using polar sampling. Our findings are as follows: **1)** Polar sampling outperforms square sampling. The accuracy curves in Fig. 2(b) show significant overall improvement compared to Fig. 2(a). For example, S-RS-5 just achieves 87.60% accuracy, whereas P-RS-5 achieves 93.92% on the entire MNIST-rot.

TABLE I: The classification accuracies on MNIST and MNIST-rot. Bold stands for best results.

Methods	Input Size	MNIST	MNIST-rot
ORN[16]	32×32	99.42%	80.01%
RotEqNet[13]	28×28	99.26%	73.20%
G-CNN[12]	28×28	99.27%	44.81%
H-Net[8]	32×32	99.19%	92.44%
B-CNN[14]	28×28	97.40%	88.29%
E(2)-CNN[11]	29×29	98.14%	94.37%
Baseline	28×28	99.43%	44.53%
SCNN	28×28	99.04%	95.05%

This aligns with our theoretical analysis in Section II-B. **2)** Ring sorting outperforms global sorting. Notably, P-RS-7 achieves the highest accuracy of 95.05%, surpassing S-RS-7’s accuracy of 92.63% by 2.42%. This is because RS partially preserves spatial information within a convolutional region. **3)** Using larger convolutional kernel sizes yields better results, especially when combined with ring sorting. For example, the accuracies obtained by P-RS-3, P-RS-5, and P-RS-7 are 88.98%, 93.92%, and 95.05%, respectively.

Fig. 2(c) and Table 1 show the classification accuracies of P-SC-7, its baseline model, and six previous rotation-invariant CNN models on the original MNIST test set and MNIST-rot. Similarly to SCNN, H-Net, B-CNN, and E(2)-CNN also have continuous rotational invariance even without data augmentation. In contrast, Oriented Response Network (ORN), RotEqNet, and G-CNN are only invariant to specific rotation angles like multiples of 30° or 45°. These models are trained using the protocols from their authors. We do not select STN [9], TI-Pooling [30], and several methods utilizing rotation-invariant loss functions [31], [32] for comparison, because their invariance relies on data augmentation. Our experimental results indicate the following: **1)** On MNIST-rot, P-SC-7 surpasses the previous state-of-the-art method, E(2)-CNN, by improving the accuracy from 94.37% to 95.05%. Additionally, the performance of P-SC-7, H-Net, B-CNN, and E(2)-CNN significantly outperforms ORN, RotEqNet, and G-CNN, highlighting the importance of achieving continuous rotational invariance in CNN models. Furthermore, due to the inability to learn rotational invariance from the training data, even though Baseline and SCNN have an equal number of learnable parameters, Baseline achieves an accuracy of only 44.53%. **2)** On the original MNIST test set, Baseline achieves the best result (99.43%). Previous research [15] has indicated that rotation-invariant CNNs struggle to distinguish between some digits, like “9” and “6”, which contributes to their slightly lower performance on this test set.

C. Results on Outex_TC_00012 and NWPU-RESISC45

We evaluate three commonly used CNN baselines and their corresponding rotation-invariant models on the Outex_TC_00012 dataset. The rotation-invariant models are obtained by replacing conventional convolutions with SC. The classification accuracy is displayed in the first column of Table II. Our rotation-invariant CNNs exhibit significantly higher accuracy compared to their baseline counterparts. For

TABLE II: The classification accuracies on Outex_TC_00012.

Training Data	24×40=1440	24×40=960	24×20=480
VGG16	60.07%	58.13%	57.36%
RI-VGG16	95.99%	92.90%	72.28%
ResNet18	64.79%	66.77%	63.10%
RI-ResNet18	99.70%	99.63%	98.41%
DenseNet40	66.02%	66.58%	60.70%
RI-DenseNet40	99.47%	98.62%	98.53%

TABLE III: The classification accuracies on NWPU-RESISC45.

Training Data	45×400=1.8K	45×300=1.35K	45×200=0.9K
VGG16	71.27%	66.32%	57.95%
RI-VGG16	78.53%	76.61%	71.39%
ResNet18	83.18%	78.99%	70.23%
RI-ResNet18	90.38%	88.45%	85.36%
DenseNet40	86.83%	84.72%	80.48%
RI-DenseNet40	88.35%	86.96%	85.93%

example, RI-ResNet18 outperforms ResNet18 by a substantial margin of 34.91%. We subsequently reduce the training set size from 1440 to 960 (only training images captured under “inca” and “t184” lighting conditions) and 480 (“inca” lighting condition only). We train six models on these smaller training sets and evaluate their performance on the original test set. The results are shown in the second and third columns of Table II. Remarkably, even when the training set excludes certain lighting conditions, RI-ResNet18 and RI-DenseNet40 achieve an accuracy of around 98.5%. This is because lighting variations do not disrupt the local structure of textures, and the rotation invariance of SC enables it to better extract essential information about local texture structures. Additionally, we conduct classification experiments on the NWPU-RESISC45 dataset, and also reduce the training set size to 1.35K and 0.9K (randomly selecting 300 and 200 images from each category, respectively). Table III presents the classification accuracies of these models on the test set. Clearly, our rotation-invariant models continue to outperform the corresponding baselines significantly, with a wider gap as the training data decreases. For instance, when the number of training images is reduced from 1.8K to 1.35K and 0.9K, the accuracy difference between RI-ResNet18 and ResNet18 increases from 7.20% to 9.46% and 15.13%, respectively.

IV. CONCLUSION

We develop a Sorting Convolution to achieve continuous rotational invariance in CNNs without additional parameters or data augmentation. Using the MNIST-rot dataset, we analyze the impact of kernel sizes, different sampling and sorting strategies on SC’s rotational invariance and compare its performance with other rotation-invariant CNNs. Further, SC can directly replace conventional convolutions in classic CNNs, improving these models’ rotational invariance. Thus, we combine SC with commonly used CNN models and conduct classification experiments on popular image datasets.

Our results show SC excels in these tasks, especially when training data is limited.

REFERENCES

- [1] D. G. Lowe. “Distinctive image features from scale-invariant keypoints,” *Int. J. Comput. Vision*, vol. 60, no. 2, pp. 91-110, 2004.
- [2] T. Ojala, M. Pietikäinen, and T. Mäenpää. “Multiresolution gray-scale and rotation invariant texture classification with local binary patterns,” *IEEE Trans. Pattern Anal. Mach. Intell.*, vol. 24, no. 7, pp. 971-987, 2002.
- [3] X. Shi, A. -L. R. Castro, R. Manduchi, and R. Montgomery. “Rotational invariant operators based on steerable filter banks,” *IEEE Signal Process. Lett.*, vol. 13, no. 11, pp. 684-687, 2006.
- [4] H. Bay, A. Ess, T. Tuytelaars, and L. V. Gool. “Speeded-up robust features (SURF),” *Comput. Vis. Image Und.*, vol. 10, no. 3, pp. 346-359, 2008.
- [5] T. Chakraborti, B. McCane, S. Mills, and U. Pal. “LOOP descriptor: local optimal-oriented pattern,” *IEEE Signal Process. Lett.*, vol. 25, no. 5, pp. 635-639, 2018.
- [6] H.-L. Mo, Q. Li, Y. Hao, H. Zhang, and H. Li. “A Rotation Invariant Descriptor Using Multi-directional and High-Order Gradients,” in *Proc. PRCV*, 2018, pp. 372-383.
- [7] M. D. Zeiler, and R. Fergus. “Visualizing and understanding convolutional networks,” in *Proc. ECCV*, 2014, pp. 818-833.
- [8] D. E. Worrall, S. J. Garbin, D. Turmukhambetov, and G. J. Brostow. “Harmonic networks: deep translation and rotation equivariance,” in *Proc. IEEE CVPR*, 2017, pp. 5028-5037.
- [9] M. Jaderberg, K. Simonyan, A. Zisserman, and K. Kavukcuoglu. “Spatial transformer networks,” in *Proc. Neural Inf. Process. Syst.(NeurIPS)*, 2015, pp. 2017-2025.
- [10] C. Esteves, C. Allen-Blanchette, X.-W. Zhou, and K. Daniilidis. “Polar transformer networks,” in *Proc. ICLR*, 2018.
- [11] M. Weiler, and G. Cesa. “General E(2)-equivariant steerable CNNs,” in *Proc. Neural Inf. Process. Syst.(NeurIPS)*, 2019.
- [12] T. Cohen, and M. Welling. “Group equivariant convolutional networks,” in *Proc. ICML*, 2016, pp. 2990-2999.
- [13] D. Marcos, M. Volpi, N. Komodakis, and D. Tuia. “Rotation equivariant vector field networks,” in *Proc. IEEE ICCV*, 2017, pp. 5048-5057.
- [14] V. Delchevalerie, A. Bibal, B. Fréney, and A. Mayer. “Achieving rotational invariance with Bessel-convolutional neural networks,” in *Proc. Neural Inf. Process. Syst.(NeurIPS)*, 2021.
- [15] H.-L. Mo, and G.-Y. Zhao. “RIC-CNN: rotation-invariant coordinate convolutional neural network,” 2022, *arXiv:2211.11812*.
- [16] Y.-Z. Zhou, Q.-X. Ye, Q. Qiu, and J.-B. Jiao. “Oriented response networks,” in *Proc. IEEE CVPR*, 2017, pp. 519-528.
- [17] M. Weiler, F. A. Hamprecht, and M. Storath. “Learning steerable filters for rotation equivariant CNNs,” in *Proc. IEEE CVPR*, 2018, pp. 849-858.
- [18] D. Laptev, N. Savinov, J. M. Buhmann, and M. Pollefeys. “TI-Pooling: transformation-invariant pooling for feature learning in convolutional neural networks,” in *Proc. IEEE CVPR*, 2016, pp. 289-297.
- [19] G. Cheng, P.-C. Zhou, and J.-W. Han. “Learning rotation-invariant convolutional neural networks for object detection in VHR optical remote sensing images,” *IEEE Trans. Geosci. Remote Sens.*, vol. 54, no. 12, pp. 7405-7415, 2016.
- [20] F. Zhang, H.-Y. Bian, Z. Lv, and Y.-F. Zhai. “Ring-masked attention network for rotation-invariant template-matching,” *IEEE Signal Process. Lett.*, vol. 30, pp. 289-293, 2023.
- [21] L. Liu, P. Fieguth, G.-Y. Kuan, and H.-B. Zha. “Sorted Random Projections for robust texture classification,” in *Proc. IEEE ICCV*, 2011, pp. 391-398.
- [22] L. Liu, P. Fieguth, D. Clausi, and G.-Y. Kuan. “Sorted random projections for robust rotation-invariant texture classification,” *Pattern Recogn.*, vol. 45, no. 6, pp. 2405-2418, 2012.
- [23] T.-C. Song, L.-L. Xin, C.-Q. Gao, G. Zhang, and T. -Q. Zhang. “Grayscale-inversion and rotation invariant texture description using sorted local gradient pattern,” *IEEE Signal Process. Lett.*, vol. 25, no. 5, pp. 625-629, 2018.
- [24] Y. LeCun, L. Bottou, Y. Bengio, and P. Haffner. “Gradient-based learning applied to document recognition,” in *Proc. IEEE*, 1998, pp. 2278-2324.
- [25] T. Ojala, T. Mäenpää, M. Pietikäinen, J. Viertola, J. Kyllönen, and S. Huovinen. “Outex-new framework for empirical evaluation of texture analysis algorithms,” in *Proc. ICPR*, 2002, pp. 701-706.
- [26] G. Cheng, J.-W. Han, and X.-Q. Lu. “Remote sensing image scene classification: benchmark and state of the art,” *Proc. IEEE*, vol. 105, no. 10, pp. 1865-1883, 2017.
- [27] K. Simonyan, and A. Zisserman. “Very deep convolutional networks for large-scale image recognition,” in *Proc. ICLR*, 2015, *arXiv preprint arXiv:1409.1556*.
- [28] K.-M. He, X.-Y. Zhang, S.-Q. Ren, and J. Sun. “Deep residual learning for image recognition,” in *Proc. IEEE CVPR*, 2016, pp. 770-778.
- [29] G. Huang, Z. Liu, L. V. D. Maaten, and K. Q. Weinberger. “Densely connected convolutional networks,” in *Proc. IEEE CVPR*, 2017, pp. 4700-4708.
- [30] D. Laptev, N. Savinov, J. M. Buhmann, and M. Pollefeys. “TI-Pooling: transformation-invariant pooling for feature learning in convolutional neural networks,” in *Proc. IEEE CVPR*, 2016, pp. 289-297.
- [31] G. Cheng, P.-C. Zhou, J.-W. Han. “Learning rotation-invariant convolutional neural networks for object detection in VHR optical remote sensing images,” *IEEE Trans. Geosci. Remote Sens.*, vol. 54, no. 12, pp. 7405-7415, 2016.
- [32] G. Cheng, J.-W. Han, P.-C. Zhou, and D. Xu. “Learning Rotation-Invariant and Fisher Discriminative Convolutional Neural Networks for Object Detection,” *IEEE Trans. Image Process*, vol. 28, no. 1, pp. 265-278, 2019.